PCCP

Cite this: *Phys. Chem. Chem. Phys.*, 2011, **13**, 18893–18904

www.rsc.org/pccp

PAPER

Formation of ultracold SrYb molecules in an optical lattice by photoassociation spectroscopy: theoretical prospects

Michał Tomza,[a] Filip Pawłowski,[ab] Małgorzata Jeziorska,[a] Christiane P. Koch[c] and Robert Moszynski*[a]

Received 15th April 2011, Accepted 29th July 2011
DOI: 10.1039/c1cp21196j

State-of-the-art *ab initio* techniques have been applied to compute the potential energy curves for the SrYb molecule in the Born–Oppenheimer approximation for the electronic ground state and the first fifteen excited singlet and triplet states. All the excited state potential energy curves were computed using the equation of motion approach within the coupled-cluster singles and doubles framework and large basis-sets, while the ground state potential was computed using the coupled cluster method with single, double, and noniterative triple excitations. The leading long-range coefficients describing the dispersion interactions at large interatomic distances are also reported. The electric transition dipole moments have been obtained as the first residue of the polarization propagator computed with the linear response coupled-cluster method restricted to single and double excitations. Spin–orbit coupling matrix elements have been evaluated using the multireference configuration interaction method restricted to single and double excitations with a large active space. The electronic structure data were employed to investigate the possibility of forming deeply bound ultracold SrYb molecules in an optical lattice in a photoassociation experiment using continuous-wave lasers. Photoassociation near the intercombination line transition of atomic strontium into the vibrational levels of the strongly spin–orbit mixed $b^3\Sigma^+$, $a^3\Pi$, $A^1\Pi$, and $C^1\Pi$ states with subsequent efficient stabilization into the $v'' = 1$ vibrational level of the electronic ground state is proposed. Ground state SrYb molecules can be accumulated by making use of collisional decay from $v'' = 1$ to $v'' = 0$. Alternatively, photoassociation and stabilization to $v'' = 0$ can proceed *via* stimulated Raman adiabatic passage provided that the trapping frequency of the optical lattice is large enough and phase coherence between the pulses can be maintained over at least tens of microseconds.

1 Introduction

Molecules cooled to temperatures below $T = 10^{-3}$ K allow for tackling questions touching upon the very fundamentals of quantum mechanics. They are also promising candidates in novel applications, ranging from ultracold chemistry and precision measurements to quantum computing. Cold and ultracold molecules are thus opening up new and exciting areas of research in chemistry and physics. Due to their permanent electric dipole moment, polar molecules are particularly interesting objects of study: dipole–dipole interactions are long range and can precisely be controlled with external electric fields. This turns the experimental parameters field strength and orientation into the knobs that control the quantum dynamics of these molecules. Hence, it is not surprising that a major objective for present day experiments on cold molecules is to achieve quantum degeneracy for polar molecules. Two approaches to this problem are being used—indirect methods, in which molecules are formed from pre-cooled atomic gases,[1–8] and direct methods, in which molecules are cooled from molecular beam temperatures, typically starting at tens of Kelvins.[9–13]

Direct cooling techniques, based on buffer gas cooling[9] or Stark deceleration,[10] produce cold molecules with a temperature well below 1 K. However, a second-stage cooling process is required to reach temperatures below 10^{-3} K. The second-stage technique which has long been thought to be the most promising is sympathetic cooling where cold molecules are introduced into an ultracold atomic gas and equilibrate with it. Sympathetic cooling has successfully been used to achieve Fermi degeneracy in ^{6}Li[14] and Bose–Einstein condensation in ^{41}K[15] and to obtain ultracold ions.[16–19] For molecular systems,

[a] *Faculty of Chemistry, University of Warsaw, Pasteura 1, 02-093 Warsaw, Poland. E-mail: robert.moszynski@tiger.chem.uw.edu.pl*
[b] *Physics Institute, Kazimierz Wielki University, pl. Weyssenhoffa 11, 85-072 Bydgoszcz, Poland*
[c] *Theoretische Physik, Universität Kassel, Heinrich-Plett-Str. 40, 34132 Kassel, Germany*

however, sympathetic cooling has not yet been attempted, and there are many challenges to overcome. In fact, calculations of the scattering cross sections for the collisions of molecules with ultracold coolant atoms suggest that sympathetic cooling may not be so very much efficient in many cases.[20–22]

Alternatively, indirect methods first cool atoms to ultralow temperatures and then employ photoassociation[4] or magnetoassociation[5] to create molecules, reaching translational temperatures of the order of a few μK or nK. In particularly fortuitous cases, photoassociation may directly produce molecules in their vibrational ground state.[7] Typically, however, the molecules are created in extremely weakly bound levels, and follow-up stabilization to the ground state is necessary. For molecules built of alkali metal atoms, this has been achieved using stimulated emission pumping[23] or alternatively, employing coherent control techniques such as Stimulated Raman Adiabatic Passage (STIRAP)[6,24–26] and vibrational cooling of molecules with amplitude-shaped broadband laser light.[27]

Closed-shell atoms such as alkali earth metals are more challenging to cool and trap than open-shell atoms such as the alkalis. Closed-shell atoms do not have a magnetic moment in their ground state that enables magnetic trapping. Moreover, for alkaline earth metals the short lifetime of the first excited ^{1}P state implies rather high Doppler temperatures, making dual-stage cooling a necessity where the second stage operates near an intercombination line. Despite these obstacles, cooling of calcium, strontium, and ytterbium atoms to micro-Kelvin temperatures has been achieved, and Bose–Einstein condensates of ^{40}Ca,[28] ^{84}Sr,[29,30] ^{86}Sr,[31] ^{88}Sr,[32] ^{170}Yb,[33] and ^{174}Yb[34] have been obtained.

In contrast to alkali metal dimers,[5] the magnetoassociation of two closed-shell atoms is not feasible experimentally even if the nuclear spin is non-zero. The zero-field splittings and couplings between the atomic threshold and molecular states provided by the largest non-zero terms in the fine structure and hyperfine structure Hamiltonian for the electronic ground state, *i.e.*, the scalar and tensor interactions between the nuclear magnetic dipole moments,[35] are simply too small.[5] On the other hand, the closed-shell structure of the alkali earth metal and ytterbium atoms leads to very simple molecular potentials with low radiative losses and weak coupling to the environment. This opens new areas of possible applications, such as manipulation of the scattering properties with low-loss optical Feshbach resonances,[36] high-resolution photoassociation spectroscopy at the intercombination line,[37,38] precision measurements to test for a time variation of the proton-to-electron mass ratio,[39] quantum computation with trapped polar molecules,[40] and ultracold chemistry.[41]

To the best of our knowledge, production of ultracold heteronuclear diatomic molecules built of closed-shell atoms has not yet been achieved experimentally. Also such processes have not yet been considered theoretically. Here we fill this gap and report a theoretical study of the photoassociative formation of heteronuclear diatomic molecules from two closed-shell atoms on the example of the SrYb molecule. Although the SrYb molecule may seem very exotic, especially for chemists, strontium and ytterbium atoms are promising candidates for producing molecules since they have both successfully been cooled and trapped. Moreover, both Sr and Yb have many stable isotopes. Such a diversity of stable isotopes is key to controlling the collisional properties of bosonic molecules with no magnetic moments and hyperfine structure. For example, one can effectively tune the interatomic interactions by choosing the most suitable isotope to achieve scattering lengths appropriate for evaporative cooling. Last but not least, we consider photoassociative formation of SrYb molecules since there are ongoing experiments[42] aiming at producing cold SrYb molecules in an optical lattice.

The plan of our paper is as follows. Section 2 describes the theoretical methods used in the *ab initio* calculations and discusses the electronic structure of SrYb in terms of the ground and excited-state potentials, transition moments, spin–orbit and nonadiabatic angular couplings. Section 3 analyzes the vibrational structure of the SrYb molecule as a prerequisite to determine an efficient route for photoassociation followed by stabilization into the vibronic ground state. It also discusses prospects of producing cold SrYb molecules by photoassociation near the intercombination line of strontium, and subsequent spontaneous or stimulated emission. Section 4 summarizes our findings.

2 Electronic structure of SrYb

In the present study we adopt the computational scheme successfully applied before to the ground and excited states of the calcium dimer[43–47] and to the $(BaRb)^+$ molecular ion.[19] The potential energy curves for the ground and excited states of the SrYb molecule have been obtained by a supermolecule method,

$$V^{2S+1|\Lambda|}(R) = E_{AB}^{SM} - E_{A}^{SM} - E_{B}^{SM}, \quad (1)$$

where E_{AB}^{SM} denotes the energy of the dimer computed using the supermolecule method SM, and E_{X}^{SM}, X = A or B, is the energy of the atom X. For the ground state potential we used the coupled cluster method restricted to single, double, and noniterative triple excitations, CCSD(T). Calculations on all the excited states employed the linear response theory within the coupled-cluster singles and doubles (LRCCSD) framework,[48] also known as the equation of motion coupled-cluster method (EOM-CCSD).[49] We refer the reader to the recent review article by Bartlett and Musiał for a detailed discussion of these *ab initio* methods.[50] The CCSD(T) and LRCCSD calculations were performed with the DALTON program.[51] Note that the methods used in our calculations are strictly size-consistent, so they ensure a proper dissociation of the electronic states, and a proper long-range asymptotics of the corresponding potential energy curves. This is especially important when dealing with collisions at ultralow temperatures, where the accuracy of the potential in the long range is crucial. The interaction potential $V^{2S+1|\Lambda|}(R)$ given by eqn (1) has a well defined asymptotics given by the multipole expansion,[52]

$$V^{2S+1|\Lambda|}(R) \approx \sum_{n=3}^{\infty} \frac{C_{2n}}{R^{2n}}, \quad (2)$$

where C_{2n} are the long-range coefficients related to the atomic properties. In the case of the SrYb molecule the asymptotic

expansion starts with the R^{-6} terms describing the dispersion interactions, but for the excited states terms describing the induction quadrupole-induced dipole contributions are also present.

For each electronic state we have computed the long-range coefficients describing the dispersion and induction interactions from the standard expressions (see, *e.g.* ref. 52 and 53) that can be derived from the multipole expansion of the interatomic interaction operator. The long-range dispersion coefficients were computed with the recently introduced explicitly connected representation of the expectation value and polarization propagator within the coupled cluster method,[54,55] and the best approximation XCCSD4 proposed by Korona and collaborators.[56] For the singlet and triplet states dissociating into Sr(^{1}P) + Yb(^{1}S), and Sr(^{3}P) + Yb(^{1}S), respectively, the dispersion coefficients were obtained from the sum-over-state expression with the transition moments and excitation energies computed with the multireference configuration interaction method limited to single and double excitations (MRCI).

The transitions from the ground $X^1\Sigma^+$ state to the $^1\Sigma^+$ and $^1\Pi$ states are electric dipole allowed. The transition dipole moments for the electric, d_i, transitions were computed from the following expression:[57]

$$d_i = \langle X^1\Sigma^+|\hat{\mathbf{d}}|(n)^1\Lambda|\rangle, \quad (3)$$

where $\hat{\mathbf{d}}$ denotes the dipole moment operator. Note that in eqn (3) $i = x$ or y corresponds to transitions to $^1\Pi$ states, while $i = z$ corresponds to transitions to $^1\Sigma^+$ states. In the present calculations the electric transition dipole moments were computed as the first residue of the LRCCSD linear response function with two electric, r, operators.[48] In these calculations we have used the DALTON program.[51] We have evaluated the dependence of the transition dipole moments with the internuclear distance for the same set of distances as the excited state potential energy curves.

The electronic states of the low lying excited states of the SrYb molecule are coupled by nonadiabatic couplings. Therefore, in this work we have computed the most important angular coupling matrix elements,

$$A(R) = \langle (n)^{2S+1}|\Lambda||L_+|\ (n')^{2S+1}|\Lambda'|\rangle. \quad (4)$$

In the above expression L_+ denotes the raising electronic angular momentum operator. Note that the electronic angular momentum operator couples states with Λ differing by one. Nonadiabatic couplings were obtained with the MRCI method and the MOLPRO code.[58] We have evaluated the dependence of the nonadiabatic coupling matrix elements with the internuclear distance for the same set of distances as the excited state potential energy curves.

Strontium and ytterbium are heavy atoms, so the electronic states of the SrYb molecule are strongly mixed by the spin–orbit (SO) interactions. Therefore, in any analysis of the formation of the SrYb molecules the SO coupling and its dependence on the internuclear distance R must be taken into account. We have evaluated the spin–orbit coupling matrix elements for the lowest dimer states that couple to the $0^{+/-}$, 1, and 2 states of SrYb, with the spin–orbit coupling operator H_{SO} defined within the Breit–Pauli approximation.[59] The spin–orbit coupling matrix elements have been computed within the MRCI framework with the MOLPRO code.[58] Diagonalization of the relativistic Hamiltonian gives the spin–orbit coupled potential energy curves for the $0^{+/-}$, 1 and 2 states, respectively. Note that all potentials in the Hamiltonian matrices were taken from CCSD(T) and LRCCSD calculations. Only the diagonal and nondiagonal spin–orbit coupling matrix elements were obtained with the MRCI method. Once the eigenvectors of these matrices are available, one can easily get the electric dipole transition moments and the nonadiabatic coupling matrix elements between the relativistic states. In order to mimic the scalar relativistic effects some electrons were described by pseudopotentials. For Yb we took the ECP28MWB pseudopotential,[60] while for Sr the ECP28MDF[61] pseudopotential, both from the Stuttgart library. For the strontium and ytterbium atoms we used spdfg quality basis sets,[61,62] augmented with a set of [2pdfg] diffuse functions. In addition, this basis set was augmented by the set of bond functions consisting of [3s3p2d1f] functions placed in the middle of the SrYb dimer bond. The full basis of the dimer was used in the supermolecule calculations and the Boys and Bernardi scheme was used to correct for the basis-set superposition error.[63]

Calculations were done for the ground state and first fifteen (eight singlet and seven triplet) excited states of SrYb. The singlet states correspond to the Sr(^{1}D) + Yb(^{1}S), Sr(^{1}P) + Yb(^{1}S), Sr(^{1}S) + Yb(4f^{13}5d6s^2), and Sr(^{1}S) + Yb(^{1}P) dissociations, while triplet states to Sr(^{3}P) + Yb(^{1}S), Sr(^{1}S) + Yb(^{3}P), and Sr(^{3}D) + Yb(^{1}S). The potential energies were calculated for twenty interatomic distances R ranging from 5 to 50 bohr for each potential curve. The ground state potential is presented in Fig. 1, while the potential energy curves for the excited states are plotted in Fig. 2. The spectroscopic characteristics of all these states are reported in Table 1. The separated atoms energy for each state was set equal to the experimental value. Numerical values of the potentials are available from the authors on request.

Before continuing the discussion of the potentials let us note that the atomic excitation energies obtained from the

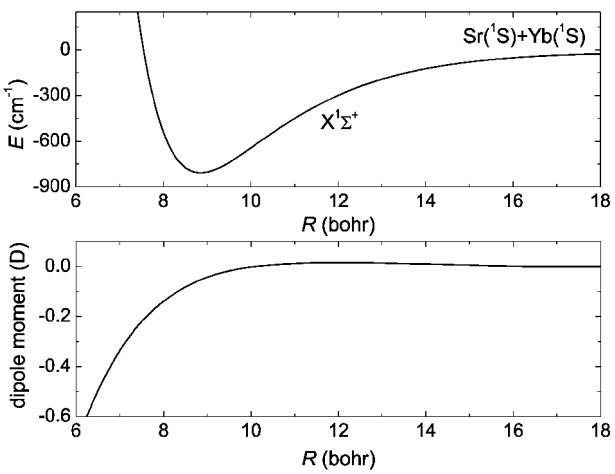

Fig. 1 Potential energy curve (upper panel) and permanent dipole moment (lower panel) of the $X^1\Sigma^+$ electronic ground state of the SrYb molecule.

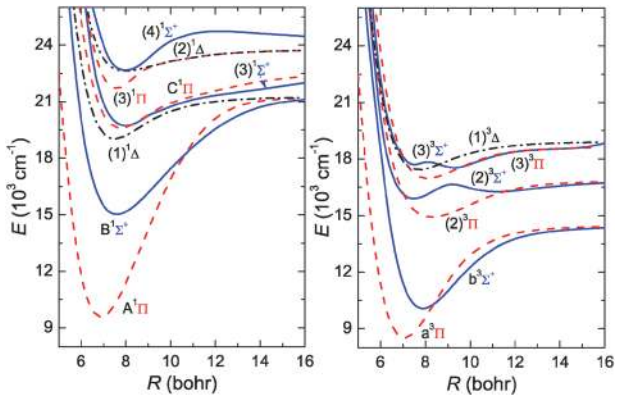

Fig. 2 Potential energy curves of singlet (left) and triplet (right) excited states of a SrYb dimer.

Table 1 Spectroscopic characteristics (equilibrium distance, well depth, harmonic constant) of the non-relativistic electronic states of the $^{88}Sr^{174}Yb$ dimer

State	R_e/bohr	D_e/cm^{-1}	ω_e/cm^{-1}	Dissociation
$X^1\Sigma^+$	8.78	828	32.8	$Sr(^1S) + Yb(^1S)$
$A^1\Pi$	6.84	11 851	94.8	$Sr(^1D) + Yb(^1S)$
$B^1\Sigma^+$	7.54	5201	63.5	$Sr(^1D) + Yb(^1S)$
$(1)^1\Delta$	7.42	1202	62.5	$Sr(^1D) + Yb(^1S)$
$(3)^1\Sigma^+$	7.91	2963	48.5	$Sr(^1P) + Yb(^1S)$
$(2)^1\Pi$	7.70	3112	61.6	$Sr(^1P) + Yb(^1S)$
$(4)^1\Sigma^+$	7.84	1790	58.6	$Sr(^1P) + Yb(\frac{7}{2},\frac{3}{2})$
$(3)^1\Pi$	7.53	2153	72.5	$Sr(^1P) + Yb(\frac{7}{2},\frac{3}{2})$
$(2)^1\Delta$	7.89	1175	40.2	$Sr(^1P) + Yb(\frac{7}{2},\frac{3}{2})$
$a^3\Pi$	7.02	6078	84.7	$Sr(^3P) + Yb(^1S)$
$b^3\Sigma^+$	7.84	4493	71.3	$Sr(^3P) + Yb(^1S)$
$(2)^3\Sigma^+$	7.39	1024	61.7	$Sr(^1S) + Yb(^3P)$
2nd min	11.02	622	21.0	
$(2)^3\Pi$	8.23	1947	42.4	$Sr(^1S) + Yb(^3P)$
$(3)^3\Sigma^+$	7.45	982	92.7	$Sr(^3D) + Yb(^1S)$
2nd min	9.33	1077	47.8	
$(3)^3\Pi$	8.04	1678	47.9	$Sr(^3D) + Yb(^1S)$
$(1)^3\Delta$	7.65	1422	50.8	$Sr(^3D) + Yb(^1S)$

CCSD calculations are accurate. Our predicted position of the nonrelativistic ^3P state of strontium is 14 463 cm^{-1}, to be compared with the experimental value of 14 705 cm^{-1}[64] deduced from the positions of the states in the P multiplet and the Landé rule. A similar accuracy is observed for the ^3D state, 18 998 cm^{-1} *vs.* 18 426 cm^{-1}. For the ^1D and ^1P states of Sr we obtain less than 5% difference with the experimental values listed by NIST.[64] Similarly good results are also obtained for the ytterbium atom. Only the ordering of the Yb ^1P and ^3D states is not reproduced correctly, but the energy difference for these states is small. Table 2 lists a comparison of the computed and experimental atomic excitation energies. We would like to stress that we computed the interaction energies according to eqn (1) using the full basis of the dimer for both the molecule and the atoms to correct the results for the basis-set superposition error, and then added the experimental atomic excitation energies. The Gaussian basis sets used in the present calculations with diffuse exponents and bond functions were optimized to get the correct description of the long-range induction and dispersion interactions, and not the atomic correlation energies. Finally we note that the lifetimes of the $^3P_1$ and $^1P_1$ states of Sr are accurately reproduced. For the $^1P_1$ state we obtained 4.92 ns to be compared with the experimental value of 5.22(3) ns.[65] For the $^3P_1$ the theoretical and experimental numbers are 22 μs and 20 μs,[38] respectively. Such a good agreement between theory and experiment for the atoms gives us confidence that the molecular results will be of similar accuracy, *i.e.* a few percent off from the exact results.

Table 2 Non-relativistic atomic excitation energies (cm^{-1})

Strontium			Ytterbium		
State	Present	Exp.[64]	State	Present	Exp.[64]
^3P	14 463	14 705	^3P	17 635	18 903
^3D	18 998	18 426	^3D	25 783	24 801
^1D	21 224	20 150	^1P	24 249	25 068
^1P	22 636	21 698	^1D	28 202	27 678

The ground $X^1\Sigma^+$ state potential energy curve is presented in Fig. 1. It follows from the naive molecular orbital theory that the SrYb molecule in the ground state should be considered as a van der Waals molecule since the molecular configuration has an equal number of bonding and antibonding electrons. No regular chemical bond is expected, except for a weak dispersion attraction and exchange-repulsion. Indeed, the ground state potential is weakly bound with the binding energy of 828 cm^{-1}. For $J = 0$ it supports $N_\nu = 62$ vibrational levels for the lightest isotope pair and up to $N_\nu = 64$ for the heaviest isotopes. The changes of the number of bound rovibrational levels and of the position of the last vibrational level for different isotopes result in changes in the sign and value of the scattering length. This should allow to choose isotopes most suitable for cooling and manipulation. The equilibrium distance, well depth, and harmonic frequency of the $X^1\Sigma^+$ state are reported in Table 1. The permanent dipole moment of SrYb in the ground electronic state as a function of the interatomic distance R is presented in Fig. 1. Except for short interatomic distances, the dipole moment is very small. This is not very surprising since the two atoms have very similar electronegativities and the charge flow from one atom to the other, after the formation of the weak van der Waals bond, is very small. In fact, similarly as the bonding of the ground state, the dipole moment of SrYb should be considered as a dispersion dipole.[66] At large interatomic distances it vanishes as R^{-6}.[67,68] The vibrationally averaged dipole moment of SrYb in the ground vibrational state is very small and equal to 0.058 D.

Potential energy curves of the excited singlet and triplet states of SrYb are presented in Fig. 2, and the corresponding long-range coefficients are reported in Table 3. The long-range

Table 3 Long-range dispersion coefficients (in a.u.) for ground and relevant excited states of the SrYb dimer

State	C_6	C_8
$X^1\Sigma^+$	2688	294 748
$A^1\Pi$	3771	502 070
$a^3\Pi$	1265	509 068
$b^3\Sigma^+$	6754	317 656

potential computed according to eqn (2) was used at distances larger than $R = 15$ bohr. A proper damping function describing the charge overlap and damping effects[52,69] was used to match the *ab initio* and the asymptotic results. The agreement between the raw *ab initio* data and the asymptotic expansion (2) with the damping effects neglected was of the order of 1% for the ground state and 3 to 4% for the excited states at $R = 15$ bohr. Inspection of Fig. 2 reveals that the potential energy curves for the excited states of the SrYb molecule are smooth with well defined minima. The potential energy curves of the (2) and $(3)^3\Sigma^+$ states show an avoided crossing and exhibit a double minimum structure. These double minima on the potential energy curves are due to strong nonadiabatic interactions between these states. Other potential energy curves do not show any unusual features, except for the broad maximum of the potential of the $(4)^1\Sigma^+$ which is most likely due to the interaction with a higher excited state not reported in the present work. Except for the shallow double minima of the $(2)^3\Sigma^+$ and $(3)^3\Sigma^+$ states, and shallow Δ states, all other excited states of the SrYb molecule are strongly bound with binding energies D_e ranging from approximately 1790 cm^{-1} for the $(4)^1\Sigma^+$ state up to as much as 11 851 cm^{-1} for the $A^1\Pi$ state.

Let us compare the potential energy curves of the heteronuclear SrYb molecule to those of the homonuclear Sr_2 dimer.[70] In general, molecular orbitals constructed from the linear combinations of the Sr(5p) + Yb(6p) or Sr(4d) + Yb(5d) atomic orbitals are expected to have less bonding or antibonding character than the molecular orbitals constructed from the Sr(5p) + Sr(5p) or Sr(4d) + Sr(4d) atomic orbitals, because large atomic orbital energy differences make combination of these orbitals less effective. This explains why many potential energy curves of the SrYb dimer are less attractive than the corresponding potential energy curves of the Sr_2 dimer. The strongly attractive character of the potential energy curves for the first $^3\Sigma^+$ and the first $^3\Pi$ states converging in the long range to $Sr(^3P) + Yb(^1S)$ asymptote could be a result of the stabilizing effect of the Yb(5d) orbitals for the lowest unoccupied orbitals of σ and π symmetry (these molecular orbitals are combinations of the Yb(6p) and Sr(5p) orbitals, but also of the appropriate Yb(5d) orbitals, closer in energy to Sr(5p)). Potential energy curves for the second $^1\Sigma^+$ and second $^1\Pi$ states converging to $Sr(^1P) + Yb(^1S)$ are less attractive than the potential energy curves for the triplet states, similarly as for the corresponding states of the Sr_2 dimer. As for the Sr_2 dimer, potential energy curves for the $^1\Sigma^+$ and $^1\Pi$ states converging to the $Sr(^1D) + Yb(^1S)$ asymptote have a much more attractive character than the triplet states converging to the $Sr(^3D) + Yb(^1S)$ asymptote.

The $a^3\Pi$, $b^3\Sigma^+$, $A^1\Pi$ and $C^1\Pi$ excited states essential for the photoassociative formation of the ground state SrYb molecule proposed in the next section are plotted in Fig. 4. The matrix elements of the spin–orbit coupling were calculated for the manifolds of coupled $a^3\Pi$, $b^3\Sigma^+$, $A^1\Pi$ states, *cf.* Fig. 3. The knowledge of the spin–orbit coupling between $a^3\Pi$, $b^3\Sigma^+$, $A^1\Pi$ and $C^1\Pi$ states allows us to obtain the relativistic $(1)0^-$, $(2)0^-$, $(1)0^+$, (1)1, (2)1, (3)1, (4)1 and (1)2 states by diagonalizing the appropriate relativistic Hamiltonian matrices. The $\Omega = 1$ states are also plotted in Fig. 4. Note that the crossing of

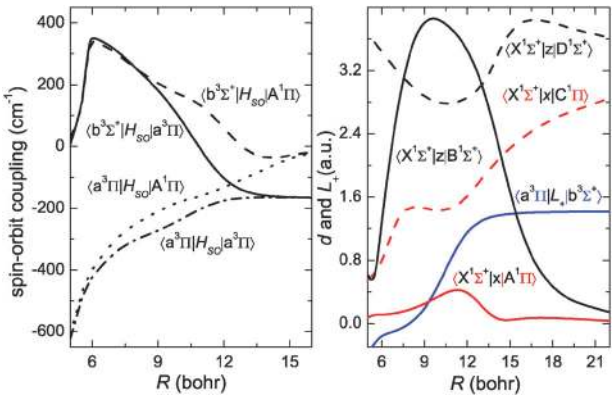

Fig. 3 Left: matrix elements of the spin–orbit interaction for the $a^3\Pi$, $b^3\Sigma^+$, and $A^1\Pi$ electronically excited states of SrYb. Right: matrix elements of the electric transition dipole moment from the $X^1\Sigma^+$ ground electronic state to $A^1\Pi$ state (solid red curve) and to the $C^1\Pi$ state (dashed red curve), and matrix elements of the nonadiabatic angular coupling between the $a^3\Pi$ and $b^3\Sigma^+$ states of SrYb (solid blue curve).

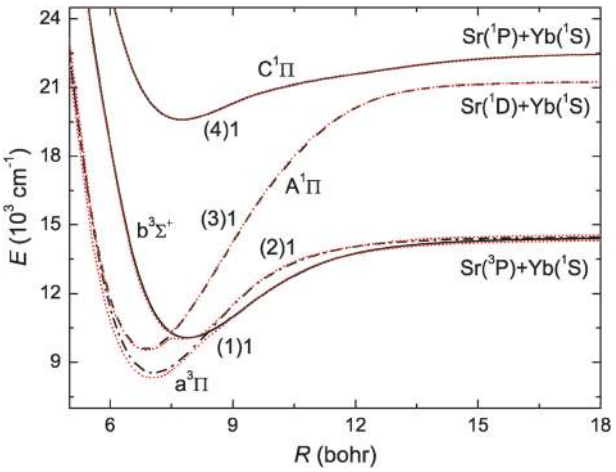

Fig. 4 The $a^3\Pi$, $b^3\Sigma^+$, $A^1\Pi$ and $C^1\Pi$ potential energy curves (solid and dashed black curves) in Hund's case (a) representation that are coupled by the spin–orbit interaction and the resulting $\Omega = 1$ relativistic states (red dotted curves) in Hund's case (c) representation of the SrYb dimer.

the $b^3\Sigma^+$ and $A^1\Pi$ nonrelativistic states becomes an avoided crossing between the (2)1 and (3)1 states.

Having all the results briefly presented above we are ready to discuss the photoassociation process of cold Sr and Yb atoms, and look for the prospects of producing ultracold SrYb molecules. To conclude this section we would like to emphasize that almost all *ab initio* results were obtained with the most advanced size-consistent methods of quantum chemistry: CCSD(T) and LRCCSD. In all calculations all electrons, except for those described by the pseudopotentials, were correlated (42 for ytterbium and 10 for strontium). Only the SO coupling matrix elements and the nonadiabatic matrix elements were obtained with the MRCI method which is not size consistent. Fortunately enough, all of the couplings are important in the region of the curve crossings or at large distances, so the effect of the size-inconsistency of MRCI on our results should not be dramatic.

3 Photoassociation and formation of ground state molecules

Photoassociation is considered for a continuous-wave laser that is red-detuned with respect to the intercombination line. This transition is dipole-forbidden. However, the $a^3\Pi$ state correlating to the asymptote of the intercombination line transition, *cf.* Fig. 4, is coupled by spin–orbit interaction to two singlet states, $A^1\Pi$ and $C^1\Pi$, that are connected by a dipole-allowed transition to the ground electronic state, $X^1\Sigma^+$. Thus an effective transition matrix element is created which can be written, to a very good approximation, as

$$d_{\mathrm{SO}}(R) = \frac{\langle X^1\Sigma^+|\hat{\mathbf{d}}|C^1\Pi\rangle\langle C^1\Pi|\hat{\mathbf{H}}_{\mathrm{SO}}|a^3\Pi\rangle}{E_{a^3\Pi} - E_{C^1\Pi}} + \frac{\langle X^1\Sigma^+|\hat{\mathbf{d}}|A^1\Pi\rangle\langle A^1\Pi|\hat{\mathbf{H}}_{\mathrm{SO}}|a^3\Pi\rangle}{E_{a^3\Pi} - E_{A^1\Pi}}, \quad (5)$$

where $\hat{\mathbf{H}}_{\mathrm{SO}}$ is the spin–orbit Hamiltonian in the Breit–Pauli approximation.[59] The long-range part of $d_{\mathrm{SO}}(R)$, dominated by the first term in the above expression, is due to the coupling with the $C^1\Pi$ state, ideally suited for photoassociation. The short-range part is due to the coupling with the $A^1\Pi$ state, paving the way toward efficient stabilization of the photoassociated molecules to the electronic ground state. The $a^3\Pi$ state, in addition to the spin–orbit coupling with the two singlet states, is also coupled to the $b^3\Sigma^+$ state correlating to the same asymptote, $Sr(^3P) + Yb(^1S)$. The Hamiltonian describing these couplings yielding Hund's case (c) $\Omega = 1$ states reads in the rotating-wave approximation

$$\hat{\mathbf{H}} = \begin{pmatrix} \hat{\mathbf{H}}^{X^1\Sigma^+} & 0 & 0 & \frac{1}{2}d_1(R)E_0 & \frac{1}{2}d_2(R)E_0 \\ 0 & \hat{\mathbf{H}}^{a^3\Pi} & \xi_1(R) & \xi_2(R) & \xi_4(R) \\ 0 & \xi_1(R) & \hat{\mathbf{H}}^{b^3\Sigma^+} & \xi_3(R) & \xi_5(R) \\ \frac{1}{2}d_1(R)E_0 & \xi_2(R) & \xi_3(R) & \hat{\mathbf{H}}^{A^1\Pi} & 0 \\ \frac{1}{2}d_2(R)E_0 & \xi_4(R) & \xi_5(R) & 0 & \hat{\mathbf{H}}^{C^1\Pi} \end{pmatrix}, \quad (6)$$

where $\hat{\mathbf{H}}^{2S+1|\Lambda|}$ is the Hamiltonian for nuclear motion in the $^{2S+1}|\Lambda|$ electronic state, $\hat{\mathbf{H}}^{2S+1|\Lambda|} = \hat{\mathbf{T}} + V^{2S+1|\Lambda|}(R) + V_{\mathrm{trap}}^{2S+1|\Lambda|}(R) - (1-\delta_{n0})\hbar\omega_{\mathrm{L}}$. The kinetic energy operator is given by $\hat{\mathbf{T}} = \hat{\mathbf{P}}^2/2\mu$ with μ the reduced mass of SrYb. The trapping potential, $V_{\mathrm{trap}}^{2S+1|\Lambda|}(R)$, is relevant only in the electronic ground state for the detunings considered below, even for large trapping frequencies. We approximate it by a harmonic potential which is well justified for atoms cooled down to the lowest trap states and corresponds to radial confinement in a 3D optical lattice. The parameters of the photoassociation laser are the frequency, ω_{L}, and the maximum field amplitude, E_0. The electric transition dipole moments are denoted by $d_1(R) = \langle X^1\Sigma^+|\hat{\mathbf{d}}|A^1\Pi\rangle$, $d_2(R) = \langle X^1\Sigma^+|\hat{\mathbf{d}}|C^1\Pi\rangle$, and the matrix elements of the spin–orbit coupling are given by

$$\xi_1(R) = \langle a^3\Pi(\Sigma = 0, \Lambda = \pm1)|\,\hat{\mathbf{H}}_{\mathrm{SO}}\,|b^3\Sigma^+(\Sigma = \pm1, \Lambda = 0)\rangle,$$

$$\xi_2(R) = \langle a^3\Pi(\Sigma = 0, \Lambda = \pm1)|\,\hat{\mathbf{H}}_{\mathrm{SO}}\,|A^1\Pi(\Sigma = 0, \Lambda = \pm1)\rangle,$$

$$\xi_3(R) = \langle b^3\Sigma^+(\Sigma = \pm1, \Lambda = 0)|\,\hat{\mathbf{H}}_{\mathrm{SO}}\,|A^1\Pi(\Sigma = 0, \Lambda = \pm1)\rangle,$$

$$\xi_4(R) = \langle a^3\Pi(\Sigma = 0, \Lambda = \pm1)|\,\hat{\mathbf{H}}_{\mathrm{SO}}\,|C^1\Pi(\Sigma = 0, \Lambda = \pm1)\rangle,$$

$$\xi_5(R) = \langle b^3\Sigma^+(\Sigma = \pm1, \Lambda = 0)|\,\hat{\mathbf{H}}_{\mathrm{SO}}\,|C^1\Pi(\Sigma = 0, \Lambda = \pm1)\rangle,$$

Σ and Λ denote the quantum numbers for the projections of electronic spin and orbital angular momenta, $\hat{\mathbf{S}}$ and $\hat{\mathbf{L}}$, onto the internuclear axis. Note that the specific shape of the $C^1\Pi$ potential energy curve as well as the R-dependence of its spin–orbit coupling and transition dipole matrix elements are not important, since the $C^1\Pi$ state provides the effective dipole coupling only at long range. We have therefore approximated the R-dependence of the couplings with the $C^1\Pi$ state by their constant asymptotic values in the calculations presented below. The Hamiltonian (6) has been represented on a Fourier grid with an adaptive step size[71–73] (using $N = 1685$ grid points and grid mapping parameters $\beta = 0.22$, $E_{\mathrm{min}} = 7 \times 10^{-9}$ hartree).

The key idea of photoassociation using a continuous-wave laser is to excite a colliding pair of atoms into a bound level of an electronically excited state.[4,74] For maximum photoassociation efficiency, the detuning of the laser with respect to the atomic asymptote, $Sr(^3P_1) + Yb(^1S)$ in our case, is chosen to coincide with the binding energy of one of the vibrational levels in the electronically excited state. Fig. 5 shows two such levels with binding energies $E_b = 5.1\ \mathrm{cm}^{-1}$ (left) and $E_b = 18.9\ \mathrm{cm}^{-1}$ (right). Since four electronically excited states are coupled by the spin–orbit interaction, the vibrational wavefunctions have components on all four electronically excited states, shown in Fig. 6(top). Note that the norm of the $C^1\Pi$-component of these two vibrational wavefunctions is smaller than 10^{-3}. Nevertheless, this is enough, similar to the photoassociation of the strontium dimers near an intercombination line,[38] to provide the transition dipole for the free-to-bound (or quasi-bound-to-bound, due to the trapping potential) excitation. The vibrational level with binding energy $E_b = 5.1\ \mathrm{cm}^{-1}$ is predominantly of triplet character (with 56% of its norm residing on the $a^3\Pi$ state, 32% on the $b^3\Sigma^+$ state and just 11% on the $A^1\Pi$ state), while the vibrational level with binding energy $E_b = 18.9\ \mathrm{cm}^{-1}$ shows a truly mixed character (55% triplet *vs.* 45% singlet). The fact that multiple

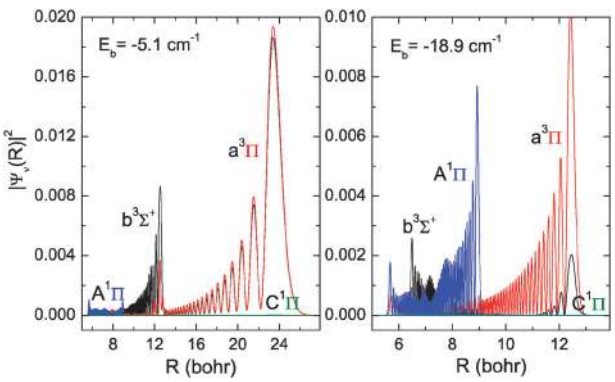

Fig. 5 Vibrational wave functions of the coupled $a^3\Pi$, $b^3\Sigma^+$, $A^1\Pi$, and $C^1\Pi$ electronic states of a SrYb molecule for two binding energies corresponding to vibrational quantum numbers $\nu' = -11$ (left) and $\nu' = -18$ (right) below the dissociation threshold.

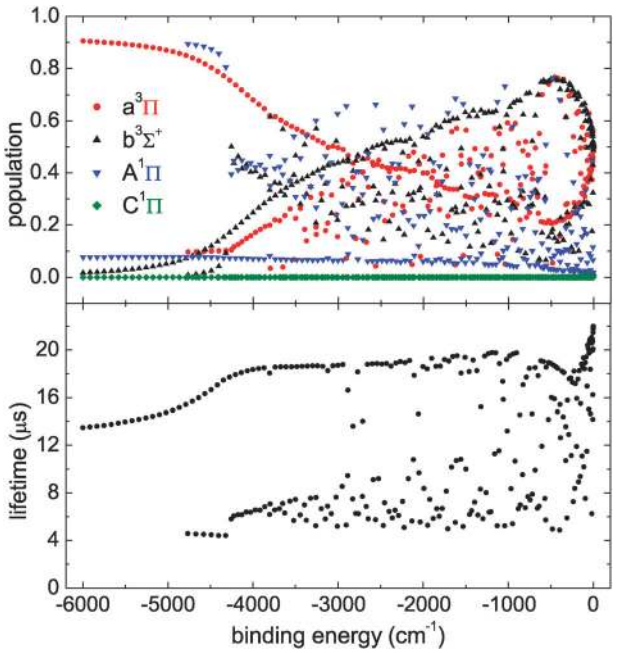

Fig. 6 Top panel: population of the $a^3\Pi$, $b^3\Sigma^+$, $A^1\Pi$ and $C^1\Pi$ components of the vibrational levels *vs.* binding energy. Bottom panel: lifetime of the vibrational levels as a function of binding energy.

classical turning points are clearly visible in the vibrational wavefunction with $E_b = 18.9\ cm^{-1}$ reflects the resonant nature of the spin–orbit coupling of this level: the coinciding energy of the levels in the coupled vibrational ladders leads to a resonant beating between the different components of the coupled wavefunctions.[75] Such a structure of the vibrational wavefunctions was shown to be ideally suited for efficient stabilization of the photoassociated molecules into deeply bound levels in the ground electronic state.[76–79]

The Condon radius for photoassociation coincides with the classical outer turning point, *i.e.*, roughly speaking with the outermost peak of the vibrational wavefunctions as shown in Fig. 5. Since the pair density of the atoms colliding in their electronic ground state decreases with decreasing interatomic distance, photoassociation is more efficient for small detuning. This is reflected by the larger values of the black compared to the red curve in Fig. 7 which shows the free-to-bound (quasi-bound-to-bound) transition matrix elements for the two vibrational wavefunctions depicted in Fig. 5 as a function of the trapping frequency of the optical lattice. The second observation to be drawn from Fig. 7 is the almost linear scaling of the transition matrix elements, and hence the photoassociation probability, with the trap frequency. That is, enhancing the trap frequency from 50 kHz, which has been employed for photoassociation of Sr_2,[38] to 500 kHz, which is within current experimental feasibility, will increase the number of photoassociated molecules by a half an order of magnitude. This confinement effect is easily understood in terms of the larger compression of the quasi-bound atom pairs in a tighter optical trap.

In view of the formation of deeply bound molecules in their electronic ground state, it might be advantageous to choose the larger detuning of $18.9\ cm^{-1}$ despite the photoassociation

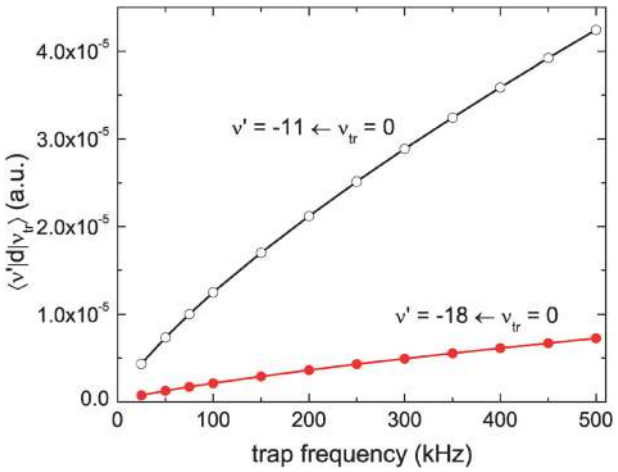

Fig. 7 Vibrationally averaged free-to-bound (or quasi-bound-to-bound) electric transition dipole moments between the lowest trap state of a pair of Sr and Yb atoms colliding in the $X^1\Sigma^+$ ground electronic state in a harmonic trap and two bound levels, *cf.* Fig. 5, of electronically excited SrYb dimers as a function of the trap frequency.

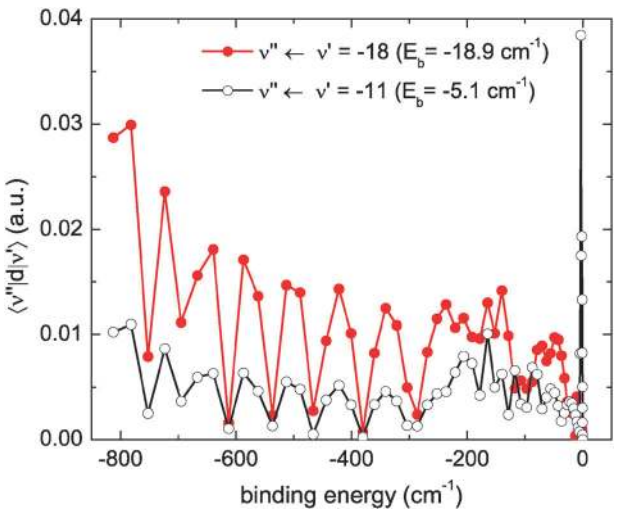

Fig. 8 Vibrationally averaged bound-to-bound electric transition dipole moments between the vibrational levels of the coupled electronically excited states that are shown in Fig. 5 and all vibrational levels of the $X^1\Sigma^+$ ground electronic state.

probability being smaller by about a factor of 5.9 compared to a detuning of $5.1\ cm^{-1}$ for all trap frequencies. This becomes evident by inspecting Fig. 8 which displays the bound-to-bound transition matrix elements between the two electronically excited vibrational wavefunctions with $E_b = 5.1\ cm^{-1}$ and $E_b = 18.9\ cm^{-1}$ and all bound levels of the $X^1\Sigma^+$ electronic ground state. These transition matrix elements govern the branching ratios for spontaneous decay of the photoassociated molecules. Note that for $\nu' = -11$ and $\nu' = -18$, the electronically excited molecules will decay into bound levels of the electronic ground state with a probability of about 24%. This decay to a large extent into bound levels is a hallmark of photoassociation near an intercombination line.[38] It is in contrast to photoassociation using a dipole-allowed transition where the probability for dissociative decay

is often several orders of magnitude larger than that for stabilization into bound ground state levels.[74] While the excited state vibrational level with $E_b = 5.1\ cm^{-1}$ has its largest transition dipole matrix elements with the last bound levels of the $X^1\Sigma^+$ ground electronic state that are only weakly bound, a striking difference is observed for the excited state vibrational wavefunction with $E_b = 18.9\ cm^{-1}$. The strong singlet–triplet mixing of this level, in particular the pronounced peak near the outer classical turning point of the $A^1\Pi$ state, *cf.* Fig. 5, leads to significantly stronger transition dipole matrix elements with deeply bound levels of the $X^1\Sigma^+$ ground electronic state for $\nu' = -18$ compared to $\nu' = -11$, the one with $\nu'' = 1$ being the largest. Of course, the transition dipole matrix elements govern not only the spontaneous decay of the photoassociated molecules but also stabilization *via* stimulated emission. Due to the comparatively long lifetime of photoassociated molecules, estimated to be of the order of 15 μs, stabilization into a selected single vibrational level of the electronic ground state can be achieved by stimulated emission using a second continuous-wave laser. The lifetimes of the excited state vibrational levels vary between 5 μs and 20 μs, *cf.* Fig. 6.† The lower limit is roughly constant as a function of binding energy while the upper limit reflects the mixing between the $a^3\Pi$ and $b^3\Sigma^+$ states. It smoothly increases from 14 μs up to 20 μs for binding energies of about 4000 cm^{-1}. The specific value of the lifetime of each level reflects its $A^1\Pi$ state character, *cf.* Fig. 6.

Before outlining how a prospective experiment forming SrYb molecules in their vibronic ground state based on our results could proceed, it is natural to ask whether the accuracy of the calculations is sufficient for such a prediction. In particular, how sensitively do our results for the binding energies and structure of the vibrational levels as well as for the transition matrix elements depend on the accuracy of the electronic structure calculations? The binding energies depend mostly on the quality of the potential energy curves, where the error is estimated to be a few percent, and to some extent, for the spin–orbit coupled excited states, on the accuracy of the spin–orbit interaction matrix elements (error of a few percent). Nevertheless, the uncertainty of our potential energy curves is smaller than the range of reduced masses, as illustrated in Fig. 9. Therefore photoassociation with subsequent stabilization to a low-lying vibrational level should work for all isotope pairs since levels with strong perturbations due to the spin–orbit interaction are always present in the relevant range of binding energies, respectively, detunings, *cf.* Fig. 9.

In fact, the exact position and the character of the excited state vibrational level, strongly perturbed such as the one with $E_b = 18.9\ cm^{-1}$ or more regular such as that with $E_b = 5.1\ cm^{-1}$ in Fig. 5, can be determined experimentally.[77,80] A possible spectroscopic signature of the character of the vibrational wavefunctions is the dependence of the rotational constants, $\langle \nu' | \frac{1}{2\mu \hat{R}^2} | \nu' \rangle$, on the binding energy of the corresponding levels. This is shown in Fig. 9 for different isotope combinations of strontium and ytterbium. The rotational constants of those

† We assume no inhomogeneous broadening to be induced by the optical lattice which can be achieved by operating the lattice at the magic wavelength.

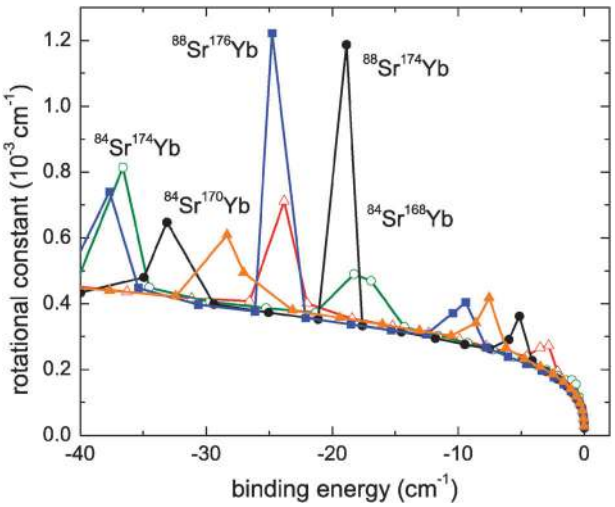

Fig. 9 Rotational constants of the vibrational levels of the coupled $a^3\Pi$, $b^3\Sigma^+$, $A^1\Pi$, and $C^1\Pi$ electronically excited states of the SrYb molecule for different isotope pairs. The isotope $^{88}Sr^{174}Yb$ was employed in the calculations shown in Fig. 5–8 and 10.

levels that are predominantly of triplet character lie on a smooth curve, while those that are mixed deviate from this curve. This behavior is easily rationalized as follows: without the coupling due to spin–orbit interaction, the rotational constants of the $a^3\Pi$, $b^3\Sigma^+$ and $A^1\Pi$ states would each lie on a smooth curve with a shape similar to the baseline of Fig. 9. The strongly mixed levels 'belong' to all three curves at the same time. Correspondingly, the value of their rotational constant lies somewhere in between the smooth curves of the regular levels. The lower peaks at small binding energies in Fig. 9 indicate mixing mostly between the $a^3\Pi$ and $b^3\Sigma^+$ states, while the higher peaks at larger binding energies reflect a strong singlet–triplet mixing. Spectroscopic determination of the rotational constants thus allows for identifying those excited state levels that show the strongest singlet–triplet mixing[77,80] and are best suited to the formation of ground state molecules. Spectroscopy is also needed to refine the value for the transition frequency of the stabilization laser. The binding energies of the deeply bound vibrational levels of the $X^1\Sigma^+$ ground electronic state come with an error of 5%, *i.e.*, $\pm 50\ cm^{-1}$, resulting from the accuracy of the electronic structure calculations. This error defines the window for the spectroscopic search.

Note that our model, eqn (6), does not account for angular couplings, *i.e.*, the couplings of the $\Omega = 1$ states with $\Omega = 0^{\pm}$ and $\Omega = 2$. When including these non-adiabatic angular couplings, we found the components of the vibrational wavefunctions on the newly coupled surfaces to account for less than 0.001% of the population. The changes in the binding energy of the vibrational levels turned out to be less than $10^{-6}\ cm^{-1}$, well within the error of the electronic structure calculations. This negligible effect of the angular (Coriolis-type) couplings for SrYb is not surprising due to its large reduced mass whose inverse enters all coupling matrix elements.

Combining all results shown above and assuming that the relevant spectroscopic data have been confirmed or adjusted experimentally, we suggest the following scheme for

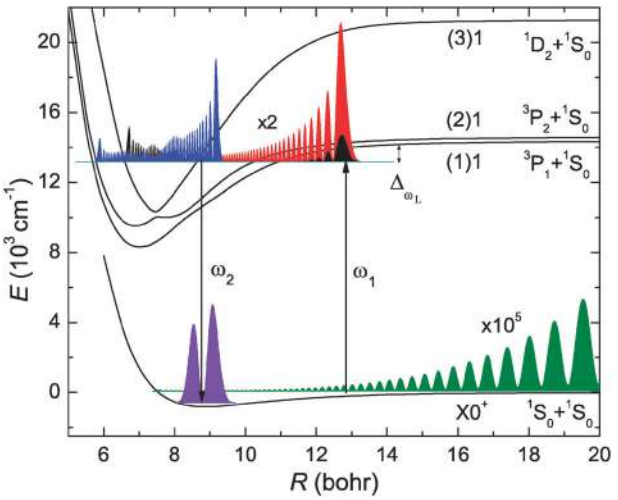

Fig. 10 Proposed scheme for the formation of ground state SrYb molecules *via* photoassociation near the intercombination line transition with detuning $\Delta_{\omega_L} = 18.9\ \mathrm{cm}^{-1}$ ($\nu_{\mathrm{trap}} = 100$ kHz).

photoassociation of SrYb dimers followed by stabilization *via* stimulated emission (see Fig. 10):

1. A large trapping frequency of the optical lattice is chosen to optimally compress the pair density of strontium and ytterbium atoms prior to photoassociation.

2. A photoassociation laser with frequency $\omega_1 \approx 690$ nm, red-detuned from the intercombination line transition and resonant with an electronically excited vibrational level, ν', of strongly mixed singlet–triplet character, is applied for a few μs. The duration of the photoassociation laser (about 5 μs roughly is an upper bound) is a compromise between saturating photoassociation and avoiding spontaneous emission losses (lifetime of about 15 μs) while the laser is on.

3. As the photoassociation laser is switched off, the stabilization laser is switched on. Due to the strong bound-to-bound transition matrix elements, saturation of the transition is expected already for shorter pulses ($\lesssim 1$ μs). The frequency of the stabilization laser, $\omega_2 \approx 655$ nm, is chosen to be resonant with the transition from the electronically excited level, ν', to the first excited vibrational level of the $X^1\Sigma^+$ electronic ground state, $\nu'' = 1$.

4. Before repeating steps 2 and 3, both photoassociation and stabilization lasers remain turned off for a hold period in which the $X^1\Sigma^+$ ($\nu'' = 1$) molecules decay to the vibronic ground state, $X^1\Sigma^+$ ($\nu'' = 0$). This ensures that the molecules created in the electronic ground state by the first sequence of the photoassociation and stabilization steps are not re-excited in a following sequence. The formed molecules can then be accumulated in $X^1\Sigma^+$ ($\nu'' = 0$).

Note that this scheme does not require phase coherence between the two pulses. Step 4 needs to involve a dissipative element in order to ensure the unidirectionality of the molecule formation scheme.[47] Dissipation can be provided by infrared spontaneous emission due to the permanent dipole moment of the heteronuclear dimers. However, this timescale is estimated to be of the order of 5 s, much too slow to be efficient for accumulation of ground state molecules. A second possibility is due to collisional decay. For the decay to occur within 1 ms, a density of 10^{13} cm^{-3} is required. Note that the density was 3×10^{12} cm^{-3} in the experiment photoassociating Sr_2 in an optical lattice with trapping frequency of 50 kHz.[38] Increasing the trap frequency will further increase the density such that hold times in the sub-ms regime are within the experimental reach.

One might wonder whether the comparatively long hold times can be avoided by using Stimulated Raman Adiabatic Passage (STIRAP)[81] for the photoassociation (pump) and stabilization (Stokes) pulses.[82,83] In order to overcome the problem of unidirectionality that occurs in repeating the photoassociation and stabilization steps many times, the whole ensemble of atom pairs in the trap needs to be addressed within a single STIRAP sweep[83] or within a single sequence of phase-locked STIRAP pulse pairs.[82] Note that the Stokes/stabilization pulse should be tuned to the $\nu' \rightarrow \nu'' = 0$ transition in this case. The feasibility of STIRAP-formation of ground state molecules depends on isolating the initial state sufficiently from the scattering continuum. A possibility to achieve this which was discussed theoretically consists in utilizing the presence of a Feshbach resonance.[83,84] If no resonance is present, *i.e.*, in an unstructured scattering continuum, STIRAP fails. In a series of ground-breaking experiments, STIRAP transfer to the ground state was therefore preceded by Feshbach-associating the molecules.[6,24–26] An alternative way to isolate the initial state for STIRAP from the scattering continuum that does not rely on Feshbach resonances (which are absent for the even isotope species of Sr and Yb) is given by strong confinement in a deep optical lattice. In a strong optical lattice the thermal spread can be made much smaller than the vibrational frequency of the trap. An estimate of the required trap frequency is given in terms of the binding energy of the Feshbach molecules that were STIRAP-transferred to the vibronic ground state. It was for example about 230 kHz for KRb molecules.[6,25] Hence a deep optical lattice with trapping frequency of the order of a hundred kHz (and corresponding temperatures $T \ll 5$ μK) should be sufficient to enable STIRAP-formation of ground state molecules. In order to be adiabatic with respect to the vibrational motion in the trap with periods of the order of about 1 μs, the duration of the photoassociation pulse needs to be rather long, at least of the order of 10 μs. The challenge might be to maintain phase coherence between the photoassociation pulse and the stabilization pulse over such timescales. For a train of phase-locked STIRAP-pulse pairs,[82] the requirement of durations of the order of 10 μs or larger applies to the length of the sequence of pulse pairs. The minimum Rabi frequencies to enforce adiabatic following are $\Omega = 159$ kHz for a 10 μs-pulse or $\Omega = 15.9$ kHz for a 100 μs-pulse. As a further prerequisite, all or at least most atom pairs should reside in the lowest trap state, $\nu_{\mathrm{trap}} = 0$. Then steps 2–4 above might be replaced, provided the trapping frequency is sufficiently large, by

2′. a single STIRAP-sweep[81] forming ground state molecules with μs-pulses where the stabilization laser, tuned on resonance with the $\nu' \rightarrow \nu'' = 0$ transition ($\omega_2 \approx 654$ nm), precedes the photoassociation laser, tuned on resonance with the $\nu_{\mathrm{trap}} = 0 \rightarrow \nu'$ transition ($\omega_2 \approx 690$ nm);

2″. or, a train of short, phase-locked STIRAP pulse pairs with correctly adjusted pulse amplitudes.[82]

To convert the Rabi frequencies to field amplitudes, note that the transition matrix elements are 5×10^{-6} for the pump pulse (assuming a trap frequency of 300 kHz) and 3×10^{-2} for the Stokes pulse. Phase coherence needs to be maintained throughout the single STIRAP-sweep or sequence of STIRAP pulse pairs.

4 Summary

Based on a first principles study, we predict the photoassociative formation of SrYb molecules in their electronic ground state using transitions near an intercombination line. The potential energy curves, non-adiabatic angular coupling and spin–orbit interaction matrix elements as well as electric dipole transition matrix elements of the SrYb molecule were calculated with state-of-the-art *ab initio* methods, using the coupled cluster and multireference configuration interaction frameworks. Assuming that the accuracy of the calculations for the SrYb molecule is about the same as for the isolated Sr and Yb atoms at the same level of the theory, we estimate the accuracy of the electronic structure data to 5%. However, the crucial point for the proposed photoassociation scheme is the existence and position of the intersection of the potential energy curves corresponding to $b^3\Sigma$ and $A^1\Pi$ states. By contrast to the binding energies of the vibrational levels, the position of this intersection does not depend very much on the overall quality of the computed potential energy curves. The correct structure of the crossings between the potential curves of the $a^3\Pi$, $b^3\Sigma$ and $A^1\Pi$ states is reproduced using even relatively crude computational methods of quantum chemistry which do not account for dynamic correlations such as the multiconfiguration self-consistent field (MCSCF) method employed here.

The spin–orbit coupled $a^3\Pi$, $b^3\Sigma^+$, $A^1\Pi$, and $C^1\Pi$ electronically excited states are essential for the photoassociation. A pair of colliding Sr and Yb atoms is excited into the triplet states ($\omega_1 \approx 690$ nm). Following stabilization by either spontaneous or stimulated emission, SrYb molecules in their electronic ground state are obtained. The required dipole coupling for photoassociation (stabilization) is provided by the $C^1\Pi$ ($A^1\Pi$) state.

If photoassociation is followed by spontaneous emission, about 24% of the photoassociated molecules will decay into bound levels of the ground electronic state, roughly independent of the detuning of the photoassociation laser. However, *which* ground state rovibrational levels are populated by spontaneous emission depends strongly on the detuning of the photoassociation laser. While most detunings will lead to decay into the last bound levels of the ground electronic states, certain detunings populate excited state levels with strong spin–orbit mixing. The strongly resonant structure of the wavefunctions allows for decay into low-lying vibrational levels. This might be the starting point for vibrational cooling[27,85] if molecules in their vibronic ground state are desired.

Alternatively, the long lifetime of the photoassociated molecules, of the order of 15 μs, allows for stabilization to the electronic ground state *via* stimulated emission, by a sequence of photoassociation and stabilization laser pulses of μs duration. Two schemes are conceivable: (i) a repeated cycle of photoassociation and stabilization pulses is applied with $X^1\Sigma^+(\nu' = 1)$ as the target level. The duration of the pulses should be of the order of 1 μs. In order to accumulate molecules in $X^1\Sigma^+(\nu = 0)$, a hold period whose duration depends on the density of atoms is required for collisional decay from $\nu = 1$ to $\nu = 0$. For deep optical lattices with corresponding high densities, hold periods in the sub-ms regime can be reached. (ii) The vibronic ground state, $X^1\Sigma^+(\nu = 0)$, is targeted directly by a counter-intuitive sequence of photoassociation and stabilization pulses (STIRAP), either using two long pulses[81] or a train of phase-locked pulse pairs.[82] The timescale for the pulses is determined by the requirement to be adiabatic with respect to the motion in the optical lattice. The largest trapping frequencies feasible to date imply pulse durations at least of the order of 10 μs. Phase coherence between the pulses needs to be maintained over this timescale. Note that STIRAP fails if applied to an unstructured scattering continuum of colliding atoms. A possibility to circumvent this is given by preselecting the initial state for STIRAP with the help of a (Feshbach) resonance.[82–84] Our variant of the scheme is different since STIRAP is enabled by the presence of a deep trap.

Before either of the above discussed molecule formation schemes can be implemented experimentally, our theoretical data need to be corroborated by spectroscopy. In particular, our binding energies come with an error of a few percent, implying a corresponding uncertainty in the transition frequencies. Moreover, the exact position of strongly spin–orbit mixed excited state wavefunctions needs to be confirmed by measuring the excited state level spacings or rotational constants. However, despite the relatively large uncertainties in the energies of the rovibrational levels important for the proposed photoassociation scheme, our *ab initio* methods correctly locate the crossing of the singlet and triplet potential energy curves. This is the key ingredient for the efficient production of ground state SrYb molecules that we are predicting with our study.

Acknowledgements

We would like to thank Tatiana Korona and Wojciech Skomorowski for many useful discussions and help with the MOLPRO program. This work was supported by the Polish Ministry of Science and Education through the project N N204 215539, and by the Deutsche Forschungsgemeinschaft (Grant No. KO 2301/2). MT was supported by the project operated within the Foundation for Polish Science MPD Programme co-financed by the EU European Regional Development Fund.

References

1 H. R. Thorsheim, J. Weiner and P. S. Julienne, *Phys. Rev. Lett.*, 1987, **58**, 2420.
2 A. J. Kerman, J. M. Sage, S. Sainis, T. Bergeman and D. DeMille, *Phys. Rev. Lett.*, 2004, **92**, 033004.
3 D. Wang, J. Qi, M. F. Stone, O. Nikolayeva, H. Wang, B. Hattaway, S. D. Gensemer, P. L. Gould, E. E. Eyler and W. C. Stwalley, *Phys. Rev. Lett.*, 2004, **93**, 243005.

4 K. M. Jones, E. Tiesinga, P. D. Lett and P. S. Julienne, *Rev. Mod. Phys.*, 2006, **78**, 483.
5 T. Köhler, K. Góral and P. S. Julienne, *Rev. Mod. Phys.*, 2006, **78**, 1311.
6 K.-K. Ni, S. Ospelkaus, M. H. G. de Miranda, A. Pe'er, B. Neyenhuis, J. J. Zirbel, S. Kotochigova, P. S. Julienne, D. S. Jin and J. Ye, *Science*, 2008, **322**, 231.
7 J. Deiglmayr, A. Grochola, M. Repp, K. Mörtlbauer, C. Glück, J. Lange, O. Dulieu, R. Wester and M. Weidemüller, *Phys. Rev. Lett.*, 2008, **101**, 133004.
8 C. Haimberger, J. Kleinert, P. Zabawa, A. Wakim and N. P. Bigelow, *New J. Phys.*, 2009, **11**, 055042.
9 J. D. Weinstein, R. de Carvalho, T. Guillet, B. Friedrich and J. M. Doyle, *Nature*, 1998, **395**, 148.
10 H. L. Bethlem, G. Berden and G. Meijer, *Phys. Rev. Lett.*, 1999, **83**, 1558.
11 H. L. Bethlem and G. Meijer, *Int. Rev. Phys. Chem.*, 2003, **22**, 73.
12 M. Schnell and G. Meijer, *Angew. Chem., Int. Ed.*, 2009, **48**, 6010.
13 S. Y. T. van de Meerakker and G. Meijer, *Faraday Discuss.*, 2009, **142**, 113.
14 B. DeMarco and D. S. Jin, *Science*, 1999, **285**, 1703.
15 G. Modugno, G. Ferrari, G. Roati, R. J. Brecha, A. Simoni and M. Inguscio, *Science*, 2001, **294**, 1320.
16 C. Zipkes, S. Palzer, C. Sias and M. Köhl, *Nature*, 2010, **464**, 388.
17 C. Zipkes, S. Palzer, L. Ratschbacher, C. Sias and M. Köhl, *Phys. Rev. Lett.*, 2010, **105**, 133201.
18 S. Schmid, A. Härter, J.H. Denschlag and A. Frisch, private communication.
19 M. Krych, W. Skomorowski, F. Pawłowski, R. Moszynski and Z. Idziaszek, *Phys. Rev. A: At., Mol., Opt. Phys.*, 2011, **83**, 032723.
20 M. Lara, J. L. Bohn, D. E. Potter, P. Soldan and J. M. Hutson, *Phys. Rev. A: At., Mol., Opt. Phys.*, 2007, **75**, 012704.
21 P. S. Żuchowski and J. M. Hutson, *Phys. Rev. A: At., Mol., Opt. Phys.*, 2009, **79**, 062708.
22 S. K. Tokunaga, W. Skomorowski, P. S. Żuchowski, R. Moszynski, J. M. Hutson, E. A. Hinds and M. R. Tarbutt, *Eur. Phys. J. D*, 2011, DOI: 10.1140/epjd/e2011-10719-x.
23 J. M. Sage, S. Sainis, T. Bergeman and D. DeMille, *Phys. Rev. Lett.*, 2005, **94**, 203001.
24 F. Lang, K. Winkler, C. Strauss, R. Grimm and J. H. Denschlag, *Phys. Rev. Lett.*, 2008, **101**, 133005.
25 S. Ospelkaus, A. Pe'er, K.-K. Ni, J. J. Zirbel, B. Neyenhuis, S. Kotochigova, P. S. Julienne, J. Ye and D. S. Jin, *Nat. Phys.*, 2008, **4**, 622.
26 J. G. Danzl, E. Haller, M. Gustavsson, M. J. Mark, R. Hart, N. Bouloufa, O. Dulieu, H. Ritsch and H.-C. Nägerl, *Science*, 2008, **321**, 1062.
27 M. Viteau, A. Chotia, M. Allegrini, N. Bouloufa, O. Dulieu, D. Comparat and P. Pillet, *Science*, 2008, **321**, 232.
28 S. Kraft, F. Vogt, O. Appel, F. Riehle and U. Sterr, *Phys. Rev. Lett.*, 2009, **103**, 130401.
29 S. Stellmer, M. K. Tey, B. Huang, R. Grimm and F. Schreck, *Phys. Rev. Lett.*, 2009, **103**, 200401.
30 Y. N. M. de Escobar, P. G. Mickelson, M. Yan, B. J. DeSalvo, S. B. Nagel and T. C. Killian, *Phys. Rev. Lett.*, 2009, **103**, 200402.
31 S. Stellmer, M. K. Tey, R. Grimm and F. Schreck, *Phys. Rev. A: At., Mol., Opt. Phys.*, 2010, **82**, 041602.
32 P. G. Mickelson, Y. N. M. de Escobar, M. Yan, B. J. DeSalvo and T. C. Killian, *Phys. Rev. A: At., Mol., Opt. Phys.*, 2010, **81**, 051601.
33 T. Fukuhara, S. Sugawa and Y. Takahashi, *Phys. Rev. A: At., Mol., Opt. Phys.*, 2007, **76**, 051604.
34 Y. Takasu, K. Maki, K. Komori, T. Takano, K. Honda, M. Kumakura, T. Yabuzaki and Y. Takahashi, *Phys. Rev. Lett.*, 2003, **91**, 040404.
35 J. Brown and A. Carrington, *Rotational Spectroscopy of Diatomic Molecules*, Cambridge University Press, 2003.
36 R. Ciuryło, E. Tiesinga and P. S. Julienne, *Phys. Rev. A: At., Mol., Opt. Phys.*, 2005, **71**, 030701.
37 S. Tojo, M. Kitagawa, K. Enomoto, Y. Kato, Y. Takasu, M. Kumakura and Y. Takahashi, *Phys. Rev. Lett.*, 2006, **96**, 153201.
38 T. Zelevinsky, M. M. Boyd, A. D. Ludlow, T. Ido, J. Ye, R. Ciuryło, P. Naidon and P. S. Julienne, *Phys. Rev. Lett.*, 2006, **96**, 203201.
39 T. Zelevinsky, S. Kotochigova and J. Ye, *Phys. Rev. Lett.*, 2008, **100**, 043201.
40 D. DeMille, *Phys. Rev. Lett.*, 2002, **88**, 067901.
41 S. Ospelkaus, K.-K. Ni, D. Wang, M. H. G. de Miranda, B. Neyenhuis, G. Qumner, P. S. Julienne, J. L. Bohn, D. S. Jin and J. Ye, *Science*, 2010, **327**, 853.
42 T. Zelevinsky, private communication, 2011.
43 B. Bussery-Honvault, J.-M. Launay and R. Moszynski, *Phys. Rev. A: At., Mol., Opt. Phys.*, 2003, **68**, 032718.
44 B. Bussery-Honvault, J.-M. Launay and R. Moszynski, *Phys. Rev. A: At., Mol., Opt. Phys.*, 2005, **72**, 012702.
45 B. Bussery-Honvault, J.-M. Launay, T. Korona and R. Moszynski, *J. Chem. Phys.*, 2006, **125**, 114315.
46 B. Bussery-Honvault and R. Moszynski, *Mol. Phys.*, 2006, **104**, 2387.
47 C. P. Koch and R. Moszynski, *Phys. Rev. A: At., Mol., Opt. Phys.*, 2008, **78**, 043417.
48 H. Koch and P. Jorgensen, *J. Chem. Phys.*, 1990, **93**, 3333.
49 H. Sekino and R. J. Bartlett, *Int. J. Quantum Chem.*, 1984, **18**, 255.
50 R. J. Bartlett and M. Musiał, *Rev. Mod. Phys.*, 2007, **79**, 291.
51 T. Helgaker, H. J. A. Jensen, P. Jorgensen, J. Olsen, K. Ruud, H. Agren, A. A. Auer, K. L. Bak, V. Bakken and O. Christiansen and *et al.*, , DALTON, *an ab initio electronic structure program, Release 2.0*, 2005.
52 B. Jeziorski, R. Moszynski and K. Szalewicz, *Chem. Rev.*, 1994, **94**, 1887.
53 R. Moszynski, in *Molecular Materials with Specific Interactions—Modeling and Design*, ed. W. Sokalski, Springer, New York, 2007.
54 B. Jeziorski and R. Moszynski, *Int. J. Quantum Chem.*, 1993, **48**, 161.
55 R. Moszynski, P. S. Żuchowski and B. Jeziorski, *Collect. Czech. Chem. Commun.*, 2005, **70**, 1109.
56 T. Korona, M. Przybytek and B. Jeziorski, *Mol. Phys.*, 2006, **104**, 2303.
57 P. R. Bunker and P. Jensen, *Molecular Symmetry and Spectroscopy*, NRC Press, Ottawa, 1998.
58 H.-J. Werner, P. J. Knowles, R. Lindh, F. R. Manby, M. Schaltz, P. Celani, T. Korona, A. Mitrushenkov, G. Rauhut and T. B. Adler and *et al.*, , *Molpro, version 2006.1, a package of ab initio programs*, 2006.
59 H. A. Bethe and E. E. Salpeter, *Quantum Mechanics of One- and Two-Electron Atoms*, Academic Press, New York, 1957.
60 M. Kaupp, P. v. R. Schleyer, H. Stoll and H. Preuss, *J. Chem. Phys.*, 1991, **94**, 1360.
61 I. S. Lim, H. Stoll and P. Schwerdtfeger, *J. Chem. Phys.*, 2006, **124**, 034107.
62 X. Cao and M. Dolg, *J. Chem. Phys.*, 2001, **115**, 7348.
63 S. F. Boys and F. Bernardi, *Mol. Phys.*, 1970, **19**, 553.
64 http://physics.nist.gov/PhysRef Data.
65 S. B. Nagel, P. G. Mickelson, A. D. Saenz, Y. N. Martinez, Y. C. Chen, T. C. Killian, P. Pellegrini and R. Côté, *Phys. Rev. Lett.*, 2005, **94**, 083004.
66 W. B. Brown and D. M. Whisnant, *Mol. Phys.*, 1973, **25**, 1385.
67 A. J. Lacey and W. B. Brown, *Mol. Phys.*, 1974, **27**, 1013.
68 T. G. A. Heijmen, R. Moszynski, P. E. S. Wormer and A. van der Avoird, *Mol. Phys.*, 1996, **89**, 81.
69 K. T. Tang and J. P. Toennies, *J. Chem. Phys.*, 1984, **80**, 3726.
70 E. Czuchaj, M. Krosnicki and H. Stoll, *Chem. Phys. Lett.*, 2003, **371**, 401.
71 V. Kokoouline, O. Dulieu, R. Kosloff and F. Masnou-Seeuws, *J. Chem. Phys.*, 1999, **110**, 9865.
72 K. Willner, O. Dulieu and F. Masnou-Seeuws, *J. Chem. Phys.*, 2004, **120**, 548.
73 S. Kallush and R. Kosloff, *Chem. Phys. Lett.*, 2006, **433**, 221.
74 F. Masnou-Seeuws and P. Pillet, *Adv. At., Mol., Opt. Phys.*, 2001, **47**, 53.
75 C. Amiot, O. Dulieu and J. Vergès, *Phys. Rev. Lett.*, 1999, **83**, 2316.
76 C. M. Dion, C. Drag, O. Dulieu, B. Laburthe Tolra, F. Masnou-Seeuws and P. Pillet, *Phys. Rev. Lett.*, 2001, **86**, 2253.
77 H. K. Pechkis, D. Wang, Y. Huang, E. E. Eyler, P. L. Gould, W. C. Stwalley and C. P. Koch, *Phys. Rev. A: At., Mol., Opt. Phys.*, 2007, **76**, 022504.

78 S. Ghosal, R. J. Doyle, C. P. Koch and J. M. Hutson, *New J. Phys.*, 2009, **11**, 055011.
79 B. E. Londoño, J. E. Mahecha, E. Luc-Koenig and A. Crubellier, *Phys. Rev. A: At., Mol., Opt. Phys.*, 2009, **80**, 032511.
80 A. Fioretti, O. Dulieu and C. Gabbanini, *J. Phys. B: At., Mol. Opt. Phys.*, 2007, **40**, 3283.
81 K. Bergmann, H. Theuer and B. W. Shore, *Rev. Mod. Phys.*, 1998, **70**, 1003.
82 E. A. Shapiro, M. Shapiro, A. Pe'er and J. Ye, *Phys. Rev. A: At., Mol., Opt. Phys.*, 2007, **75**, 013405.
83 E. Kuznetsova, P. Pellegrini, R. Côté, M. D. Lukin and S. F. Yelin, *Phys. Rev. A: At., Mol., Opt. Phys.*, 2008, **78**, 021402.
84 E. Kuznetsova, M. Gacesa, P. Pellegrini, S. F. Yelin and R. Côté, *New J. Phys.*, 2009, **11**, 055028.
85 A. Bartana, R. Kosloff and D. J. Tannor, *Chem. Phys.*, 2001, **267**, 195.

